Neurobiology of Disease 124 (2019) 67–80

Contents lists available at ScienceDirect

Neurobiology of Disease

journal homepage: www.elsevier.com/locate/ynbdi

Gallic acid disruption of $A\beta_{1-42}$ aggregation rescues cognitive decline of APP/PS1 double transgenic mouse

Mei Yu[a], Xuwei Chen[a], Jihong Liu[b], Quan Ma[a], Zhan Zhuo[a], Hao Chen[a], Lin Zhou[a], Sen Yang[a], Lifeng Zheng[a], Chengqing Ning[c], Jing Xu[c], Tianming Gao[b], Sheng-Tao Hou[a,*]

[a] Brain Research Centre and Department of Biology, Southern University of Science and Technology, 1088 Xueyuan Blvd, Nanshan District, Shenzhen, Guangdong Province 518055, PR China
[b] Key Laboratory of Psychiatric Disorders of Guangdong Province, Southern Medical University, Guangzhou 510515, PR China
[c] Department of Chemistry, Southern University of Science and Technology, 1088 Xueyuan Blvd, Nanshan District, Shenzhen, Guangdong Province 518055, PR China

ARTICLE INFO

Keywords:
Alzheimer's disease
Gallic acid
Amyloid-β-aggregation
Morris water maze
Novel object recognition test
Y-maze
LTP
Ratiometric calcium imaging
Molecular docking

ABSTRACT

Alzheimer's disease (AD) treatment represents one of the largest unmet medical needs. Developing small molecules targeting Aβ aggregation is an effective approach to prevent and treat AD. Here, we show that gallic acid (GA), a naturally occurring polyphenolic small molecule rich in grape seeds and fruits, has the capacity to alleviate cognitive decline of APP/PS1 transgenic mouse through reduction of $A\beta_{1-42}$ aggregation and neurotoxicity. Oral administration of GA not only improved the spatial reference memory and spatial working memory of 4-month-old APP/PS1 mice, but also significantly reduced the more severe deficits developed in the 9-month-old APP/PS1 mice in terms of spatial learning, reference memory, short-term recognition and spatial working memory. The hippocampal long-term-potentiation (LTP) was also significantly elevated in the GA-treated 9-month-old APP/PS1 mice with increased expression of synaptic marker proteins. Evidence from atomic force microscopy (AFM), dynamic light scattering (DLS) and thioflavin T (ThT) fluorescence densitometry analyses showed that GA significantly reduces $A\beta_{1-42}$ aggregation both *in vitro* and *in vivo*. Further, pre-incubating GA with oligomeric $A\beta_{1-42}$ reduced $A\beta_{1-42}$-mediated intracellular calcium influx and neurotoxicity. Molecular docking studies identified that the 3,4,5-hydroxyle groups of GA were essential in noncovalently stabilizing GA binding to the Lys28-Ala42 salt bridge and the –COOH group is critical for disrupting the salt bridge of $A\beta_{1-42}$. The predicated covalent interaction through Schiff-base formation between the carbonyl group of the oxidized product and ε-amino group of Lys16 is also critical for the disruption of $A\beta_{1-42}$ S-shaped triple-β-motif and toxicity. Together, these studies demonstrated that GA can be further developed as a drug to treat AD through disrupting the formation of $A\beta_{1-42}$ aggregation.

1. Introduction

Alzheimer's disease (AD) is the most common form of senile dementia affecting millions of people worldwide. Characterized by the gradual loss of cognitive functions due to abnormal deposition of extracellular fibrillary amyloid beta peptides (Aβ) and intracellular neurofibrillary tangles in the brain (Kalaria et al., 2008; Korczyn, 2008), it has been hypothesized that targeting Aβ neurotoxicity is a potentially effective method to treat AD (Barrett et al., 2010; Herline et al., 2018; Kayed et al., 2011; Mori et al., 2017; Wisniewski and Drummond, 2016). A substantial amount of studies has shown that larger Aβ aggregates are not responsible for neurodegeneration. It is the smaller soluble oligomers that are the toxic species of Aβ (Du et al., 2015; Sengupta et al., 2016). The intermediate structures of aggregated Aβ which is formed earlier than plaques are the cause of pathogenesis seen in AD (Sengupta et al., 2016; Hardy and Selkoe, 2002). Because oligomeric $A\beta_{1-42}$ is the most toxic to neurons, it is suggested that an effective amyloid fibril inhibitor should target the β-sheet secondary structure rather than the primary structure. Therefore, any inhibitors which can prevent fibril formation are likely to be effective against disease-related fibril-forming proteins (Liu et al., 2013; Nesi et al., 2017).

The $A\beta_{1-42}$ fibril is the predominant constituent of amyloid plaques, while $A\beta_{1-40}$ are more abundant in the plasma (Gravina et al., 1995). The observation that $A\beta_{1-42}$ oligomers form calcium conducting channels in the neuronal bilayer membranes (Demuro et al., 2005; Demuro

* Corresponding author.
E-mail address: hou.st@sustc.edu.cn (S.-T. Hou).

https://doi.org/10.1016/j.nbd.2018.11.009
Received 4 July 2018; Received in revised form 8 November 2018; Accepted 12 November 2018
Available online 14 November 2018
0969-9961/

et al., 2010) led to the search for small molecules inhibiting calcium channels (Diaz et al., 2009). Both nonspecific Aβ channel blockers, such as trimethamine (Tris) and Zn^{2+}, and selective blockers, such as MRS2481 and an enatiomeric species MRS2485, have been shown to inhibit Aβ neurotoxicity (Diaz et al., 2009; Forner et al., 2017; Kocis et al., 2017). Glutamate receptors, including NMDA type and AMPA type receptors, are also involved in Aβ neurotoxicity through increased Ca^{2+} influx (Demuro et al., 2010). Drugs like memantine targeting glutamate receptor-mediated intracellular Ca^{2+} influx have been developed to provide neuroprotection to treat mid- to late-stage AD (Chen and Lipton, 1997; Lipton and Chen, 2004). Thus, calcium homeostasis plays critical roles in the mechanisms of Aβ-induced neurotoxicity (Bezprozvanny and Mattson, 2008; Mattson et al., 1992).

Small molecules from polyphenolic compounds, such as gallic acid (GA; 3,4,5-trihydroxybenzoic acid) widely existed in many fruits and teas, are reported in the literature as inhibitors for assembly of Aβ fibrils *in vitro* (LeVine 3rd et al., 2012). GA rapidly decreases fibril-dependent Thioflavine T (ThT) fluorescence of aggregated $Aβ_{1–40}$ through a mechanism of stabilizing preformed soluble oligomers and without competing for ThT binding. It is suggested that GA may remodel toxic Aβ oligomers into nontoxic species (LeVine 3rd et al., 2012). Additionally, GA also efficiently inhibits *in vitro* aggregation and toxicity of α-synuclein, amyloid fibril formation of insulin and kappa-casein which spontaneously form amyloid fibrils (Di Giovanni et al., 2010; Jayamani and Shanmugam, 2014; Kroes et al., 1992; Liu et al., 2013). GA also possesses other properties, such as scavenging free radicals, anti-oxidation (Kim et al., 2011; Kim, 2007), and anti-inflammation (Kroes et al., 1992), which may also contribute to the protective effect of GA against AD.

Despite of these studies, very little is known regarding pharmacological and cognitive behavioral benefits of GA *in vivo*. Most of the published studies used *in vitro* cultured cells or systems of low physiological relevance to AD (Ferruzzi et al., 2009; Hajipour et al., 2016; Jayamani and Shanmugam, 2014; Kim et al., 2011; Kim, 2007; Kroes et al., 1992; Liu et al., 2013). For example, a study showed that GA corrected LTP deficits in rat after injection of $Aβ_{1–42}$ (Hajipour et al., 2016). This model is highly unphysiological. Information on GA's effect on cognitive behavior in a more physio-pathological relevant *in vivo* model system, such as the APPswe/PS1dE9 double transgenic mouse (APP/PS1), is not available. Mori and colleagues used a combination of octyl gallate and ferulic acid to show improvement in cognition and neurodegeneration in APP/PS1 mouse. Because octyl gallate can be efficiently transformed to GA in the intestine, it has been postulated that octyl gallate's effect was due to GA (Mori et al., 2017). To firmly establish GA as a potential lead for development as therapeutics for AD treatment, a direct demonstration of GA's efficacies in cognition and behavior is necessary.

To this end, we used transgenic APP/PS1 as a model system to examine the efficacies of GA on cognitive behavioral changes. APP/PS1 mouse develops Aβ deposits much earlier than the single transgenic mouse (Kurt et al., 2001). Widespread Aβ plaques with or without a distinct core occur in both the gray and white matters. The 4-month-old and 9-month-old APP/PS1 mice were used to represent the low plaque and high plaque load stages, respectively, during AD development. Experimental data indicated that GA provided protection through disruption of $Aβ_{1–42}$ fibril formation. Collectively, our results provided new evidence to show that GA can indeed enhance cognitive behavior *in vivo*, and that GA effectively reduces the aggregation of $Aβ_{1–42}$ and neurotoxicity, thereby serving as a good lead for the development as a therapeutic drug against AD.

2. Materials and methods

2.1. Preparation of $Aβ_{1–42}$

Synthetic human $Aβ_{1–42}$ (> 95%) was purchased from GL Biochem (Shanghai, China) and prepared as preciously described (Ittner et al., 2010). Briefly, fresh $Aβ_{1–42}$ powder was dissolved in 1,1,1,3,3,3-Hexafluoro-2-propanol (HFIP, Fluka, USA) to achieve a final concentration of 1 mM. The solution was left in quiescence for 1 h at room temperature, which was then distributed into aliquots in new centrifuge tubes with opened lids for evaporation at room temperature for about 3 h. Afterwards, it was followed by drying in a speed-vac concentrator (CentriVap® Concentrator, Labconco, USA) at 37 °C for 1 h. The lyophilized peptides were stored at −20 °C until use. To obtain oligomeric $Aβ_{1–42}$, the HFIP-treated peptides was re-dissolved in DMSO to a concentration of 2.5 mM and sonicated in a water bath for 5 min. The solution was then diluted in Dulbecco's Modified Eagle Medium/Nutrient Mixture F-12 to 100 μM and incubated for 48 h at 4 °C. After that, the solution was centrifuged at 12000 rpm for 10 min at 4 °C, and the supernatant was collected for the subsequent experiment.

To produce aggregated $Aβ_{1–42}$ (Du et al., 2015), the HFIP-treated $Aβ_{1–42}$ peptides was re-dissolved in 10 mM NaOH to a concentration of 2.5 mM and sonicated in a cold water bath for 30 min, followed by dilution in PBS to the required concentration. The solution was incubated for 3 days at 37 °C to form aggregated $Aβ_{1–42}$.

2.2. Neuronal viability assay using CCK8 kit

Neuronal viability was assessed with a cell viability counting kit – 8 purchased from BBI Life Sciences (Shanghai, China). Briefly, primary cortical neurons treated with $Aβ_{1–42}$ for the specified period of time and the amount were collected following the manufacturer's protocol. Exactly 100 μL of cell suspension was transferred to a 96-well plate at a final concentration of 500,000 cells/mL. Cells were incubated with 10 μL CCK-8 solution from the kit per well for 4 h and assessed with a Perkin-Elmer spectrometer (EnSpire, Perkin-Elmer, USA) at the absorbance of 450 nm.

2.3. Quantification of Aβ plaques using Thioflavin S staining

Thioflavin S staining of frozen brain sections was performed as previously described with minor modifications (Ittner et al., 2010). Briefly, mouse brain was fixed in 4% paraformaldehyde for 48 h and dehydrated in 10% and 30% sucrose solution. Coronal sectioning at 10 μm thickness of mouse brain with 10 serial sections was performed in a cryostat. Brain sections were dried in the air and dehydrated in ethanol solution. Brain sections were incubated with 1% thioflavin solution, diluted in the 80% of ethanol, for 15 min. The sections were then washed with ethanol and stained with DAPI. The green fluorescence of thioflavin S stained plaques were visualized with a Zeiss M2 upright microscope. The number of Aβ plaques were counted within the same size field of view in $μm^2$ under the microscope. Quantitative densitometry analysis was performed using Image J (NIH, Version 1.43u) to semi-quantitatively compare the density of Aβ plaques in the brain.

2.4. Primary cortical neuron culture and imaging

Primary cortical neuron culture was performed as previously described, with minor modifications (Hou et al., 2013, 2006, 2016, 2015; Jiang et al., 2007). Briefly, E15 embryonic mouse cerebral cortex was treated with papain (P3125-10MG, sigma) dissolved in Neurobasal® Media (Gibco, USA) for 30 min at 37 °C to dissociate cortices into single cells. Cells were then resuspended in neurobasal media containing trypsin inhibitor. Tissues not sufficiently digested were removed after a brief centrifugation. Fully separated cortical neurons in the supernatant were collected and plated at 5×10^4 cells/mL in 6-well (4 mL/well), 24-well (1 mL/well), or 96-well (100 μL/well) plates (Corning, NY). Neurons were cultured at 37 °C in a humidified atmosphere of 5% CO_2 for 7–8 days before use.

Cells were observed using a Leica SP8 confocal microscope. A z-

series of images were captured using 63× oil immersion objective and photos were captured under 1024 × 1024 pixel resolution and 488 nm laser light with system-optimized *Z*- steps and interval length. Dendrites of around 20 to 30 neurons were imaged in each group. Then the image series were reconstructed using NIH ImageJ (Image → stacks → Z project → Max Intensity) and analyzed using a NeuronStudio software. For every neuron, 150 μm to 200 μm secondary dendrite segments were selected randomly for dendritic spine number counting.

2.5. Ratiometric measurement of $[Ca^{2+}]i$ using Fura-2

Ratiometric calcium imaging was performed on neurons to detect intracellular calcium level as we have previously described (Han et al., 2013; Hou et al., 2006, 2016). Briefly, cortical neurons on coverslips in 24 well plates were treated with Fura-2-AM fluorescence dye (molecular probes®, Life Technologies, USA) in a final concentration of 5 μL/mL, and incubated at 37 °C with 5% CO_2 for 20 min. After rinsing twice with 37 °C PBS Mg^{2+}-free buffer, the coverslips were transferred into a new 35 mm dish containing 3 mL PBS Mg^{2+}-free buffer. Fura-2 fluorescence was measured at 510 nm emission with 340/380 nm dual excitation selected by a DG-5 system (Sutter Instrument Company, Novato, CA) and imaged with fluorescence microscope (Leica DMI4000B, Germany). The intracellular calcium ($[Ca^{2+}]i$) concentration was expressed as ratios from fluorescence intensity between the two excitation wavelengths of R340/380 of Fura-2. Mg^{2+}-free buffer containing 45 mM KCl was applied to neurons to induce $[Ca^{2+}]i$ in order to confirm neuronal membrane potential and viability following all treatments. All measurements were independently repeated for at least 3 times. For each experiment, at least 30 neurons were selected for analysis.

2.6. Thioflavin T (ThT) fluorescence assay

Thioflavin T (ThT) fluorescence is used regularly to quantify the formation and inhibition of amyloid fibrils in the presence of anti-amyloidogenic compounds such as polyphenols. Thioflavin T (ThT) assay was performed as previously described with minor modifications (Hudson et al., 2009). Briefly, $A\beta_{1-42}$ powder was dissolved in 1 mL 1,1,1,3,3,3-Hexafluoro-2-propanol (HFIP), sonicated for 5 min to completely dissolve the $A\beta_{1-42}$, followed by incubation for 1 h at room temperature, and aliquoted into 1.5 mL microcentrifuge tubes. HFIP in each tube was completely evaporated over 3 h in a fume hood, followed by evaporation for 1 h in a SpeedVac concentrator (CentriVap® Concentrator, Labconco, USA) at the room temperature. To produce aggregated $A\beta_{1-42}$, the HFIP-treated $A\beta_{1-42}$ peptides was re-dissolved in 10 mM NaOH and sonicated in cold water bath for 30 min, diluted to a final concentration of 25 μM in PBS (pH 7.4). The $A\beta_{1-42}$ solution was incubated for 3 d at 37 °C to form aggregated $A\beta_{1-42}$.

$A\beta_{1-42}$ fibrils at 20 μM concentration were mixed with different concentrations of GA. The mixture was added into a 96-well plate at 200 μL/well, followed by incubating with 10 μM ThT for 15 min at 37 °C before recording. Fluorescence from ThT was detected using a Perkin-Elmer Luminescence spectrometer (EnSpire™ Multilabel Reader, Perkin-Elmer, Singapore). Excitation and emission wavelengths for fluorescence spectroscopy were at 450 nm and 485 nm, respectively.

2.7. Dynamic light scattering (DLS) assay

DLS measurements were performed using a Zetasizer Nano S (Malvern Instruments, Worcestershire, UK) according to the method described in (Kim, 2007). For *in situ* measurements, autocorrelation functions of scattered light were collected using acquisition times of 3 min and converted into particle-size distributions using the “narrow modes” or “general purpose” algorithms provided with the Zetasizer Nano S. Changes in scattering intensity were derived from the count rates of the avalanche photodiode photon detector.

2.8. DLS measurements

Aggregation state of $A\beta_{1-42}$ with the presence of GA was further determined using DLS technique. The hydrodynamic radius (Rh) measurements were taken at 90° angle and 637 nm on Brookhaven BI-200SM. All samples ($A\beta_{1-42}$ fibrils at 20 μM and GA at 40 μM) were filtered through a 0.22 μM pore sized micro filter (Millex-GP, SLGP033RB) and placed directly into a quartz cuvette. Data collection was done at a physiological temperature (37 °C). The mean Rh and the polydispersity (Pd) were calculated from the autocorrelation analysis of light intensity data (> 40 acquisitions) based on the diffusion coefficients, which can be converted by the Stokes−Einstein equation.

2.9. Atomic force microscopy (AFM)

$A\beta_{1-42}$ solution at 10 μL volume was loaded on freshly cleaved, unmodified AFM grade mica surface (Electron Microscopy Sciences, cat. No. 71856-01-10, USA). Samples were incubated with mica for 10 min and rinsed with 5 drops of deionized water to remove buffer salts and unbound peptides. The mica surface was blow-dried under a gentle stream of nitrogen. The AFM experiments were conducted in tapping mode in air on an MFP-3D Infinity AFM (Asylum Research, Oxford Instruments) at room temperature.

2.10. Animal model of AD

All animal experiments were approved by the Animal Ethics Committee of the Southern University of Science and Technology (Shenzhen, China). APPswe/PS1dE9 (referred to as APP/PS1) transgenic mice were gifts from the nstitute of Neuroscience at Shanghai (Chinese Academy of Sciences). These mice with a C57BL/6 background express chimeric amyloid precursor protein (APPswe) encoding the Swedish mutations at amino acids 595/596 and an exon-9-deleted human PS1 (PS1dE9) controlled by independent mouse prion protein promoter elements (Jankowsky et al., 2001). Both of the genetic modifications are associated with familial AD in humans (Haass et al., 1995). The APP/PS1 mouse was generated by co-injecting two vectors encoding the human mutant APP and PSEN1 to produce elevated Aβ levels (Kurt et al., 2001). At the age of 4-month-old, these mice begin to develop small amount of Aβ plaque deposition and show working memory deficits (Lagadec et al., 2012).

Mice were maintained in a SPF II animal facility with controlled environment (temperature: 22 ± 1 °C; humidity: 50 ± 10%, and a 12 h light/dark cycle). Mice were allowed food and water *ad libitum*. These mice were bred with C57BL/6 mice to establish a colony of APP/PS1 mice and wildtype littermates. Genotyping of mice was carried out using tail tip DNA following the standard DNA extraction and PCR protocol.

2.11. Gallic acid administration

We used APP/PS1 and their wildtype littermates to examine whether GA could ameliorate AD pathology and cognitive deficits *in vivo*. GA treatment was given to both the 4-month-old group and the 9-month-old groups. GA was dissolved in sterile water at the concentration of 3 mg/mL, and was given to mice daily at 30 mg/kg through gavage as previously described (Kim et al., 2011). Repeated dosing of GA has been found to be effective in rats (Ferruzzi et al., 2009). Sterile water was given to mice serving as a vehicle-treated control group. All mice were weighed every week in the morning. After GA treatment, mice were subjected to a suite of behavioral tests.

2.12. Mouse behavioral tests

2.12.1. Open field test

After the last GA administration, mice spontaneous activity in the

open field were tested using a clear plastic cube box (41 × 41 × 38 cm) under a camera, the center region was defined as a 20 cm × 20 cm virtual area. Each mouse was given 10 min to move freely in the box. All traveled distances and the distance trace center was recorded and analyzed using Smart V3.0, Panlab software. The rearing number, representing the number of times mouse lifting the forepaws to explore upwards, was recorded by the experimenter.

2.12.2. Morris water maze (MWM)

Morris water maze was performed to determine the spatial learning ability and reference memory. MWM was performed in a blue water pool (120 cm in diameter with 2/3 of transparent water) containing a circular bright blue platform (14 cm in diameter and submerged 1.5 cm beneath the water surface).

2.12.2.1. Spatial acquisition test. The spatial acquisition learning ability training consisted of five consecutive days of training with every training day comprising of four trials with 15 min inter-trial interval. The entry points randomly selected each time from the different designated locations. Once mouse successfully found the platform within 60 s, it was placed into a cage under a warming lamp. Otherwise, mouse was gently and manually guided to the platform and allowed to remain there for at least 20 s. The traveled distance to platform was recorded in each day to assess the spatial learning ability.

2.12.2.2. Probe trial test. On day 6, a probe trial test was performed. The hidden platform was removed from the pool and the mouse was placed in the quadrant diagonally opposite the target quadrant and allowed to swim for 60 s. The time spent in the target quadrant and mean distance to target were recorded and analyzed as a measure of spatial memory retention (or the reference memory) (Vorhees and Williams, 2006). Mice were monitored by a camera and its trajectory was analyzed using the Smart V3.0, Panlab software.

2.12.3. Y-maze spontaneous alternations

To assess spatial working memory of the mice, spontaneous alternation behavior was assessed in a Y maze after the MWM. The Y maze used in this test was composed of three identical acrylic light blue arms (31 cm long, 17 cm high and 9.5 cm wide). During each trial, mouse was placed at the maze center and allowed to explore freely through the maze for 5 min. The sequence of arm entries was recorded by a monitor right above the apparatus and analyzed using the Smart V3.0, Panlab software. Alternation percentage (%) was calculated as a proportion of arm choices differing from the previous two choices (Hughes, 2004).

2.12.4. Novel object recognition test

The novel object recognition test was carried out to assess the short-term recognition memory after the Y maze test. The task was adapted to the experimental setting as described previously (Leger et al., 2013). Each trial of a mouse consisted of a familiarization session and a test session. In the familiarization session, each mouse was individually placed into an open field testing box, mouse was allowed to explore freely for 10 min in the box with two identical objects on the symmetrical diagonal position. One hour after the familiarization, one familiarized object in the box was replaced with a novel object having different brightness, shape and texture. In the test session, mouse was put back into the box again and given 5 min to explore the two different objects. The activity of the mice was recorded using Noldus video tracking system (Ethovision). Duration of time was recorded to represent basic tendency of the mouse to sniff and explore novelty objects when the mouse nose point was around the object (distance between the nose and the object was < 2.5 cm). Discrimination index was defined as the ratio of exploration duration around the novel object over duration around both the objects in the test session.

In order to minimize the difference made by experimenter handling, throughout all behavioral experiments, mice were handled by the same one experimenter.

2.13. Electrophysiological recordings of long-term potentiation (LTP)

The method used to obtain LTP was essentially based on a previously described protocol (Han et al., 2013; Liu et al., 2015). The transverse hippocampal slices (400 μm) were prepared using a Vibrotome slicer (VT 1000S; Leica) in ice-cold artificial cerebral spinal fluid (aCSF). The composition of aCSF was (in mM): 120 NaCl, 2.5 KCl, 1.2 NaH_2PO_4, 2.0 $CaCl_2$, 2.0 $MgSO_4$, 26 $NaHCO_3$, and 10 glucose, saturated with 95% O_2/5% CO2 (*v*/v). After incubating for 30 min at 34 °C and 2–8 h at the room temperature (25 ± 1 °C), the hippocampal slice was kept submerged in aCSF (3 mL/min; 32–34 °C) with a nylon mesh. The same aCSF that injected into the glass pipettes (1–5 MΩ) was used to record the field potential, field excitatory postsynaptic potentials (fEPSPs) evoked in the CA1 stratum radiatum by stimulating Schaffer collaterals (SC) with a two-concentrically bipolar stimulating electrode. The evoked responses were recorded in current-clamp mode by the Axon MultiClamp 700B (Molecular Devices) amplifier. Stimulation intensity was adjusted to evoke fEPSP amplitudes that were 25% of maximal response. LTP was induced by applying one or four trains of high-frequency stimulation (HFS: 50 pulses in 100 Hz, and an inter-train interval of 10 s, stimulation at test stimulus intensity).

2.14. GA binding docking modeling

All GA derivatives were purchased from Sigma Aldrich. GA derivatives binding and interaction with $A\beta_{1-42}$ were examined using Molecular Operating Environment (MOE) 2014.09 software at the atomic level (Scholz et al., 2015). Crystal structure of fibrillar $A\beta_{1-42}$ (PDB: 2MXU) was downloaded from PDB website, and was structure-prepared using Protonate 3D program in MOE. Induced fit was selected as the docking protocol, and Amber12: EHT was selected as the force-field. The other settings were selected as default options. The docking results were scored based on London dG scoring function and the top one was selected for binding analysis.

2.15. Golgi-Cox immersion staining and dendritic spine analysis

The brain left hemispheres were collected for Golgi-cox staining using a rapid GolgiStain™ kit (FD NeuroTechnologies, Ellicott City, MD, USA). The procedures used were exactly as described in the supplier's manual. Briefly, brains samples were rinsed with double-distilled H_2O (ddH_2O) and then immersed in the mixture solution of 1:1 volumetric ratio of FD impregnation solution mixture of A:B for two weeks at room temperature in the dark. The impregnation solution was then replaced once after 24 h of immersion. After impregnation, brains were transferred to FD solution C and stored in dark for five days. Solution C was replaced once after 24 h incubation. Afterwards, brain sample was mounted on specimen disc with optimum cutting temperature compound (Sakura Finetek, Inc., Torrance, CA, USA). Snap freeze and cryosectioning were performed on a Leica CM1950. Coronal sections of 200 μm thickness were cut and transferred to 24-well plate with ddH_2O. Brain sections were rinsed twice with ddH_2O and stained solution E (solution E: ddH_2O = 1:1:2) for 10 min. After rinsing twice in ddH_2O, sections were dehydrated in series of ascending concentrations of ethanol. Brain sections were finally cleared with xylene, mounted onto LabServ positively charged slides and sealed with resinous mounting medium (Neutral balsam, Sinopharm Chemical Reagent Co. Ltd., Shanghai, #10004160).

Dendritic spine analysis: Images used for analysis of dendritic spines were acquired using confocal microscope (Leica, LPS8) *via* z-stack series acquisition. Analyzed image series at the same spot were converted into minimized signal stack through NIH ImageJ in Z project (version 1.8.0). Pyramidal neurons in the frontal neocortex were imaged (Coordinates: Bregma 0.0 to +0.8 mm, Interaural +3.80 to +4.60 mm). Secondary

dendrites and beyond were analyzed and at least three dendritic segments longer than 10 μm were analyzed in each neuron. The measurements for basal and apical dendrites were performed separately. Subsequent analysis of these images was carried out on a software Reconstruct (http://synapses.clm.utexas.edu). Length of each imaged dendritic segment was measured through Z trace and corresponding spines were identified and counted by three independent investigators in a double-blind manner. For each neuron, the final spine densities were averaged from results obtained by three investigators.

2.16. Statistical analysis

All data were represented as mean ± SEM. One-way ANOVA plus LSD *post hoc* analysis were employed to analyze the data obtained from body weight measure, probe trial test of MWM, OFT, Y maze, NORT, quantification of Aβ plaques. A repeated measure ANOVA was applied to the analysis of traveled distance to platform in the spatial acquisition test of MWM in order to detect significant differences between groups at different days. For this test, LSD *post hoc* test was performed. For the LTP recordings, neuronal viability and ratiometric measurement of $[Ca^{2+}]i$ data analyses, one-way ANOVA plus Tukey's *post hoc* analysis was used. All analyses were performed using SPSS 22.0 software. A p value < .05 was taken to indicate statistical significance.

3. Results

3.1. GA alleviates cognitive impairments of 4-month-old AD mouse

To determine the possible beneficial effect of GA in the early stage of AD development, 4-month-old APP/PS1 transgenic mice were given GA through gavage for 30 d at 30 mg/kg/d (Fig. 1A). The drug dosage and route of delivery were chosen based on a previous report of similar animal studies (Kim et al., 2011) and our *in vitro* studies. Mice were randomly assigned into four groups (n = 6–9 per group): WT group, wildtype mice; WT + GA group, wildtype mice treated with GA; APP/PS1 group, AD transgenic mice; and APP/PS1 + GA group, AD transgenic mice treated with GA (Fig. 1). All groups of mice were monitored for physiological changes during the period of oral administration of GA: (1) Mice were weighed every week to confirm no significant changes in body weight (Supporting Fig. S1A). (2) The open field test (OFT) was performed at the end of the last GA oral administration to monitor the spontaneous activity of GA-treated mice. All four groups showed no significant differences (Supporting Fig. S1B–D). Cerebral blood flows of all groups were measured using Moor FLPI-2 (full-field laser perfusion imager) to exclude the possibility that GA may affect cerebral blood flow (Supporting Fig. S6). These experiments indicated that GA treatment did not have a major negative impact on mouse normal brain physiology.

Subsequently, a battery of behavioral tests was carried out on these mice as depicted in Fig. 1. Behavioral tests included Morris water maze test (MWM), novel object recognition test (NORT) and the Y maze test. As shown in Fig. 1B, the spatial acquisition profiles of all 4 groups of mice were similar with a gradual shortening of path length to platform measurements over the 5 d spatial acquisition training period. These results demonstrated that the spatial learning abilities of APP/PS1 transgenic mice were comparable to those of the WT littermates. But, in the subsequent day 6 of spatial probe trial test, the APP/PS1 transgenic mice group exhibited mild deficit in memory retention as shown by the appearance of more random location searches, a longer mean distance of path length to target ($p < 0.01$, Fig. 1C), and a lesser amount of time spent in the target quadrant ($p < 0.01$, Fig. 1D) compared to the WT littermate mice. By contrast, GA-treated group of APP/PS1 mice (APP/PS1 + GA group) spent significantly more amount of time in the target quadrant ($p < 0.05$, Fig. 1D) compared with those of APP/PS1 group. These data demonstrated that GA improved the spatial reference memory deficit in the young AD mice.

In addition, NORT was performed which showed no significant differences amongst all groups in the discrimination index, indicating clear preferences for the exploration of novel objects during the test session (Fig. 1E). In contrast, Y-maze test, which evaluates spatial working memory, showed that the APP/PS1 group exhibited a significantly lower alternation behavior than the WT group ($p < 0.001$, Fig. 1F), confirming deficits in remembering which arm was explored. This alternation behavior deficit was significantly ameliorated in the APP/PS1 + GA group ($p < 0.05$, Fig. 1F), demonstrating that GA was effective in enhancing spatial working memory during the early stage of AD development.

To confirm the selectivity and specificity of GA's effect, a GA derivative called benzoic acid (for its structure, see Fig. 7A) was given to 4-month-old APP/PS1 mice using gavage, which showed no improvement in cognitive behavior in MWM, Y Maze, NORT and OFT tests (Supporting Fig. S3). To demonstrate that both GA and BA can indeed get into the brain after gavage, both peripheral blood and brain samples were collected after 1, 6, 12, and 24 h after gavage for mass spectrometry analysis. As shown in Supporting Fig. S4, GA and BA level peaked after 1 h of gavage and stayed elevated in the brain and blood up to 6 h.

3.2. GA alleviates cognitive impairments of 9-month-old AD mouse

To determine whether GA can also reduce the more severe cognitive deficits of AD mice at a relatively late stage, the 9-month-old APP/PS1 transgenic mouse was given GA orally through gavage for 30 d at 30 mg/kg/d. The treatment schema is shown in Fig. 1A, which was identical to that used for the 4-month-old mice. Again, no major changes in the body weight occurred in both GA-treated WT and APP/PS1 mice as shown in the Supporting Fig. S5A (body weight measurements). Based on OFT data, the 9-month-old APP/PS1 mice showed more exploratory activities, representing increased anxiety compared to the WT littermates (Supporting Fig. S5B–D). Interestingly, GA treatment reduced this behavior in APP/PS1 mice as shown in the Supporting Fig. S5 B–D.

The 9-month-old APP/PS1 mice exhibited significant cognitive impairments before GA treatment (Fig. 1G–K). The spatial learning ability of APP/PS1 mice was significantly impaired based on the spatial acquisition trials of the MWM test (Fig. 1H, $p < 0.05$ on the 3rd and 4th d, $p < 0.01$ on the 5th d). Poor memory retention with a longer mean distance of path length to target (Fig. 1I, $p < 0.001$) and a lesser time spent in target quadrant (Fig. 1J, $p < 0.01$) occurred in APP/PS1 mice during the probe trial tests when compared with those of the WT group. Remarkably, GA treatment of APP/PS1 transgenic mice significantly enhanced the acquisition of spatial learning ability compared to APP/PS1 group (Fig. 1G, # indicates $p < 0.05$; ## indicates $p < 0.01$). GA-treated APP/PS1 mice also showed better memory retention in the probe trials than the untreated APP/PS1 mice (Fig. 1H and I). These data indicated that GA can mitigate the spatial learning and reference memory deficits in late stage of AD development.

The discrimination index of the APP/PS1 mice in the NORT test showed significant reduction compared with that of the WT mice (Fig. 1J, $p < 0.05$). After GA administration, the percentage of recognition index was significantly enhanced in the GA-treated APP/PS1 group (Fig. 1J, $p < 0.05$). Moreover, the alternation percentage of APP/PS1 group was significantly reduced compared with WT group and APP/PS1 + GA group in the Y-maze test (Fig. 1K, $p < 0.01$ with WT *vs.* APP/PS1; $p < 0.05$ in APP/PS1 *vs.* APP/PS1 + GA). These findings suggested that GA was effective in enhancing both the short-term recognition memory and the spatial working memory in the high plaque load stage of AD mice.

3.3. GA improves synaptic strength of the 9-month-old AD mice

LTP is widely considered as one of the major cellular mechanisms that underlies learning and memory. To understand GA's mechanism in

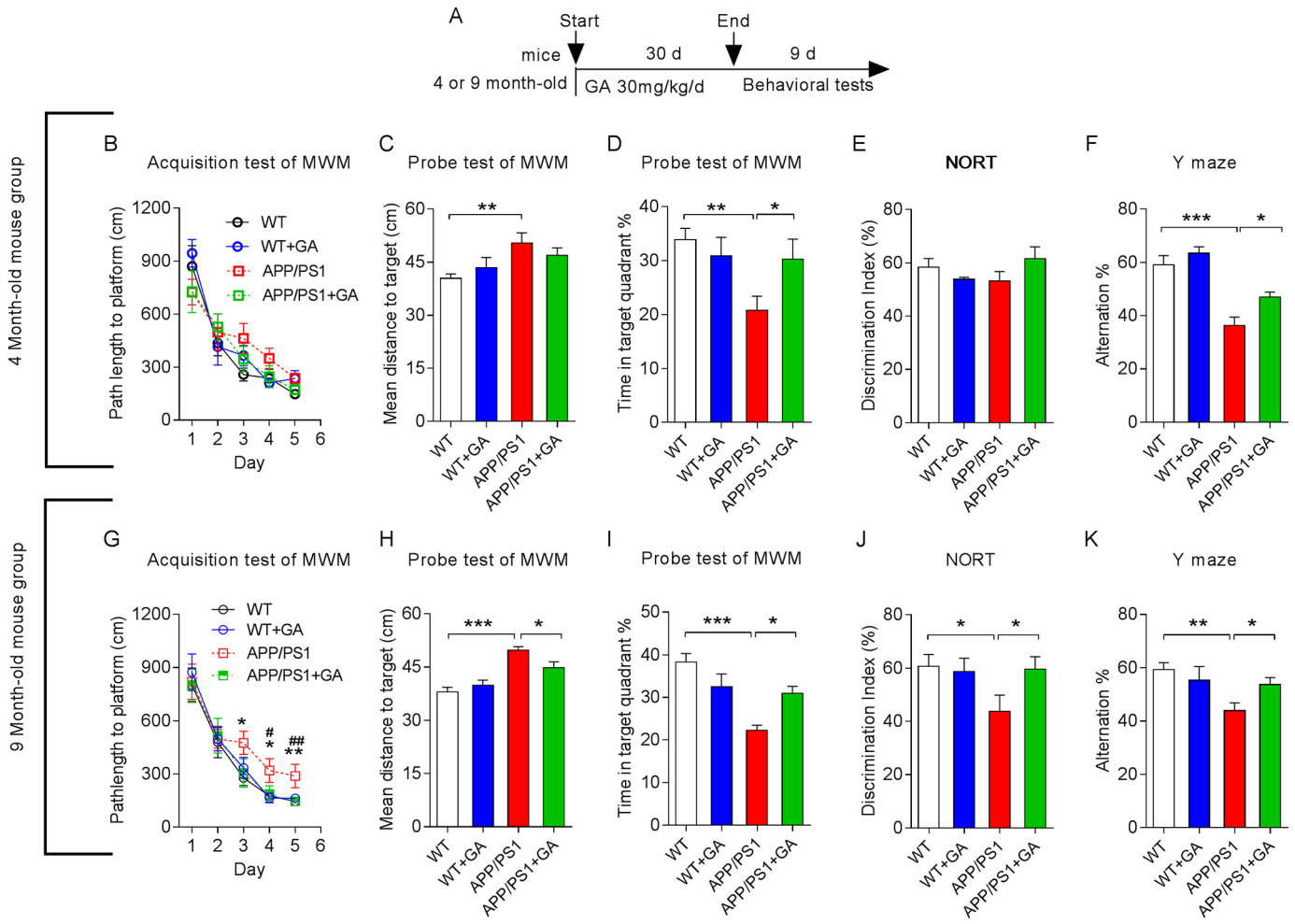

Fig. 1. GA alleviated the cognitive impairment in APP/PS1 mice. (A) Experimental design: Starting at 4 or 9 months of age, WT littermates and APP/PS1 transgenic mice were administrated with GA through oral gavage at 30 mg/kg/day for 1 month, followed by a battery of behavioral tests lasting for 9 days. Behavioral tests included MWM (B-D; G-I), NORT (E, J), Y-maze (F, K). (B and G): the acquisition tests of the MWM. Mean path-length to the platform was calculated for each day at the spatial acquisition stage of MWM of all four groups of mice. (C and H): Mean distance to the target, and (D and I): Percentage of time spent in the target quadrant during the spatial exploring stage of MWM are shown. (E and J): The percentage of exploration time spent on the novel object in the test session (NORT), expressed as a discrimination index. (F and K): The percentage of spontaneous alternation in Y maze was recorded and calculated. Data represent mean ± SEM. Error bars indicate SEM (n = 6–10 mice in each group). * $p < 0.05$, ** $p < 0.01$, *** $p < 0.001$ (one-way ANOVA with Tukey's *post hoc* analysis to identify significant groups).

enhancing spatial learning and memory, electrophysiological recordings of LTP in response to GA treatment were performed. High frequency tetanic stimulation of the Schaffer collaterals projected to the CA1 pyramidal neurons in acute hippocampal slices established the baseline synaptic responses of the 10-month-old WT and APP/PS1 littermate mice (9-month-old AD mice plus 1 month GA treatment). The input/output (I/O) curves of field excitatory postsynaptic potentials (fEPSP) slope with series of increasing stimulation intensities were shown in Fig. 2A. Comparing the basal synaptic transmission between the WT littermates with APP/PS1 mice showed no statistically significant difference (Fig. 2A).

However, LTP generated in the 10-month-old APP/PS1 group of mice was significantly reduced compared to the WT littermate group of mice (Fig. 2B and C; $p < 0.001$ with WT potentiation at 150.86 ± 3.33% *vs.* APP/PS1 potentiation at 104.29 ± 4.81%), confirming the development of severe deficits in synaptic strength associated with learning and memory in the 10-month-old APP/PS1 mice. Remarkably, APP/PS1 + GA group significantly augmented the normalized slope of fEPSP compared with that of the APP/PS1 mouse group (Fig. 2B and C; $p < 0.001$ with APP/PS1 + GA group potentiation at 143.23 ± 3.75% *vs.* APP/PS1 potentiation at 104.29 ± 4.81%), suggesting GA treatment led to the enhancement of synaptic strength in APP/PS1 mice.

Indeed, results of Western blotting of hippocampal proteins showed that the expression level of PSD95 and synaptophysin (not shown) proteins also increased significantly in GA-treated groups (Fig. 3A, B; $p < 0.05$), indicating strengthening of synapses. Interestingly, GA-treated brains showed reduced expression of GFAP, but increased expression of IBA1 compared with the non-treated group, indicating the reduced inflammatory astrocytosis following GA treatment. This may indirectly contribute to the enhancement of synaptic strength seen on LTP.

To further demonstrate the role of GA in synaptic plasticity, Golgi staining was performed on brain sections (Fig. 3C, D). The number of apical dendritic spines were counted (Fig. 3D). APP/PS1 mice at 9-month-old showed significantly reduced dendritic spine numbers compared to the wild-type littermates. GA treatment increased the numbers of the dendritic spines of APP/PS1 mouse neurons, albeit by a small margin compared to the vehicle-treated APP/PS1 mice ($p = 0.04$). Using an acute neuronal injury model where cultured neuronal cells (Fig. 3E) were treated with $A\beta_{1-42}$ for 24 h in the presence or absence of GA (Fig. 3F and G, respectively), no significant

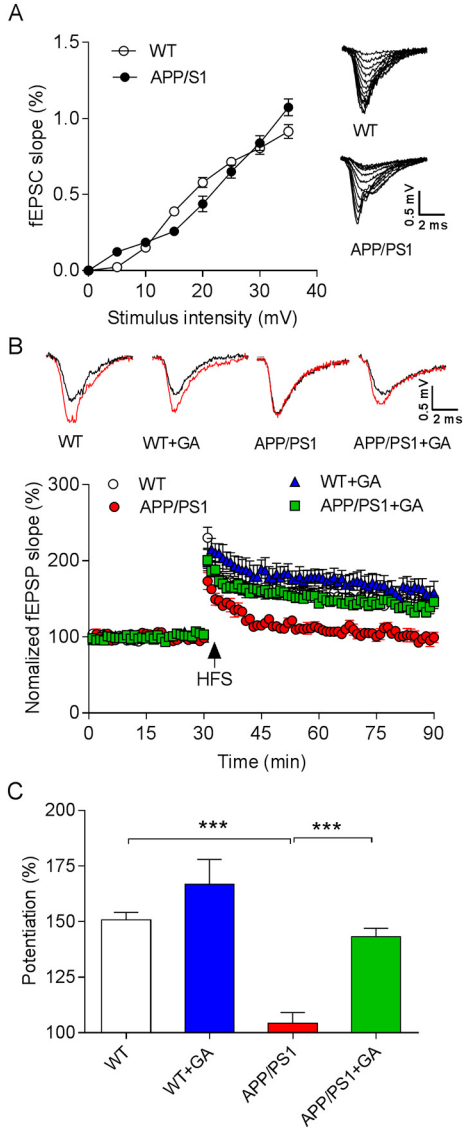

Fig. 2. GA treatment significantly improved the synaptic strength of 10-month-old APP/PS1 mice. APP/PS1 mice at 9-month-old was given GA for 1 month before recording. The LTP was generated by high frequency tetanic stimulation (HFS) of the Schaffer collaterals projected to the CA1 pyramidal neurons on acute hippocampal slices from the 10-month-old APP/PS1 mice. (A) Input/output [IO] curves of fEPSP (mV/ms) *versus* stimulation intensity (mV) were taken from the wild-type littermate and APP/PS1 mice. The changes fEPSPs slopes of the four groups over the time course are shown in panel (B). The first 20 min of evoked responses were normalized and used as the baseline responses of LTP. (C) The magnitude of LTP was determined according to the responses between 45 and 60 min after the HFS. Data represent mean ± SEM. Error bars indicate SEM (n = 5–6 mice in each group). *** $p < 0.001$.

rescue of the reduction in dendritic spines caused by $A\beta_{1-42}$ occurred (Fig. 3H), indicating that this model may not be relevant for the study of GA effect.

3.4. Gallic acid reduces Aβ plaque size, not numbers, in APP/PS1 mouse brain

To determine whether GA reduces Aβ load in treated mouse brain, brain sections were stained either with thioflavin S (ThS) which selectively labels Aβ plaques (Fig. 4A), or with an amyloid plaque specific antibody 6E10 (Supporting Fig. S7). First, APP/PS1 mice showed a significantly increased numbers of Aβ plaques in the CA1, DG and cerebral cortex regions (Fig. 4A–D; $p < 0.01$). There were no Aβ plaques found in the CA3 region (not shown). After 1 month of GA treatment of the 9-month-old APP/PS1 mice (APP/PS1 + GA group), the number of plaques per mm^2 area in the hippocampal CA1 and DG regions remained unchanged compared to that of the GA-treated APP/PS1 mice (Fig. 4B, C), except for the numbers of Aβ plaques in the cerebral cortex, which showed significant reduction in the GA- treated APP/PS1 mice group (Fig. 4D). Interestingly, the average size of Aβ plaques was significantly reduced in APP/PS1 + GA group compared with those of the APP/PS1 group in the CA1, DG and cerebral cortex regions (Fig. 4E–G; $p < 0.01$). A specific antibody to Aβ plaques 6E10 (Abcam) was also used on these sections which showed a similar pattern of reduction in Aβ plaque size confirming ThS studies (Supporting Fig. S7). Together, these findings indicated that GA shrank the size of Aβ aggregation and potentially prevented plaque formation in the brain.

3.5. Gallic acid decreases $A\beta_{1-42}$ aggregation and neuronal death in vitro

To further investigate the possibility that GA reduces Aβ aggregation, the following four *in vitro* experiments were performed as shown in Fig. 5. First, thioflavin T (ThT) fluorescence densitometry assay was used to quantify GA-mediated reduction in ThT positive Aβ fibrils. At the concentration ratio of 1:2 (Aβ:GA) and to a lesser extend at 1:1 (Aβ:GA), GA significantly reduced ThT fluorescence over time in solution (Fig. 5A).

Second, dynamic light scattering (DLS) was used to determine the size distribution profile of Aβ particles in solution suspension. Adding GA to the aggregated $A\beta_{1-42}$ fibrils (Fig. 5B) for 2 h clearly reduced the $A\beta_{1-42}$ fibril particle size from predominantly 100 nm fibrils (blue colored bars) to about 60 nm sized particles (red colored bars).

Third, the atomic force microscopy (AFM) technique was used to show GA reduction of preformed aggregated $A\beta_{1-42}$ fibrils (Fig. 5C). The top panels of Fig. 5C showed that incubation of 2.5 μM $A\beta_{1-42}$ at 4 °C for 2 d and followed by incubation at 37 °C for 1 h, 1 d, or 7 d will develop clear Aβ fibrils of different sizes and structures as seen under the AFM. Incubating $A\beta_{1-42}$ at 4 °C for 2 d and followed by incubation at 37 °C for 1–7 d had clearly increased the development of fibrillary structures. Interestingly, the toxicity of these Aβ particles were very different. Neuronal toxicities of these formed particle were shown in each panel on the left-hand side corner in black boxes. It is clear that $A\beta_{1-42}$ particles shown in the first three top panels have the highest toxicity to neurons in cultures at 33.25 ± 1.21%, 51.77 ± 0.94%, 45.9 ± 2.43%, respectively. In contrast, the top last panel showed the highest degree of $A\beta_{1-42}$ fibril formation and the least degree of neuronal toxicity (5.05% ± 1.84%). The bottom panels of Fig. 5C showed that when GA at 5 μM concentration was added with 2.5 μM $A\beta_{1-42}$ at 37 °C for 1 h or 1–7 d clearly reduced the fibril sizes of $A\beta_{1-42}$ particles. Neuronal toxicity was also reduced accordingly as shown by the numbers in the black-colored boxes in the lower panels of Fig. 5C ($p < 0.01$ by Student's t-test when compared with the corresponding top panels).

Fourth, moreover, cultured cortical neurons were preincubated with GA for 15 min before the addition of oligomeric forms of $A\beta_{1-42}$ ($A\beta_{1-42}$ at 2.5 μM at 4 °C for 2 d and 37 °C for 1 h with aggregation stage corresponding to Fig. 5C top 2nd panel). At this condition, $A\beta_{1-42}$ at 2.5 μM concentration killed 51.77% ± 0.94% of cultured cortical neurons over 24 h period (Fig. 5D), while in contrast, GA at 1 and 5 μM concentrations provided significant neuroprotection against $A\beta_{1-42}$ toxicity (Fig. 5D; $p < 0.001$). GA was not effective in preventing glutamate induced neuronal death (Fig. 4D, last bar). Glutamate-induced neurotoxicity and MK801 protection against glutamate toxicity were used as internal controls (Fig. 5D).

Taken together, these data clearly demonstrated that GA can effectively reduce $A\beta_{1-42}$ fibril aggregation formation and neurotoxicity, which serves to explain the mechanism of GA's effect in neuroprotection.

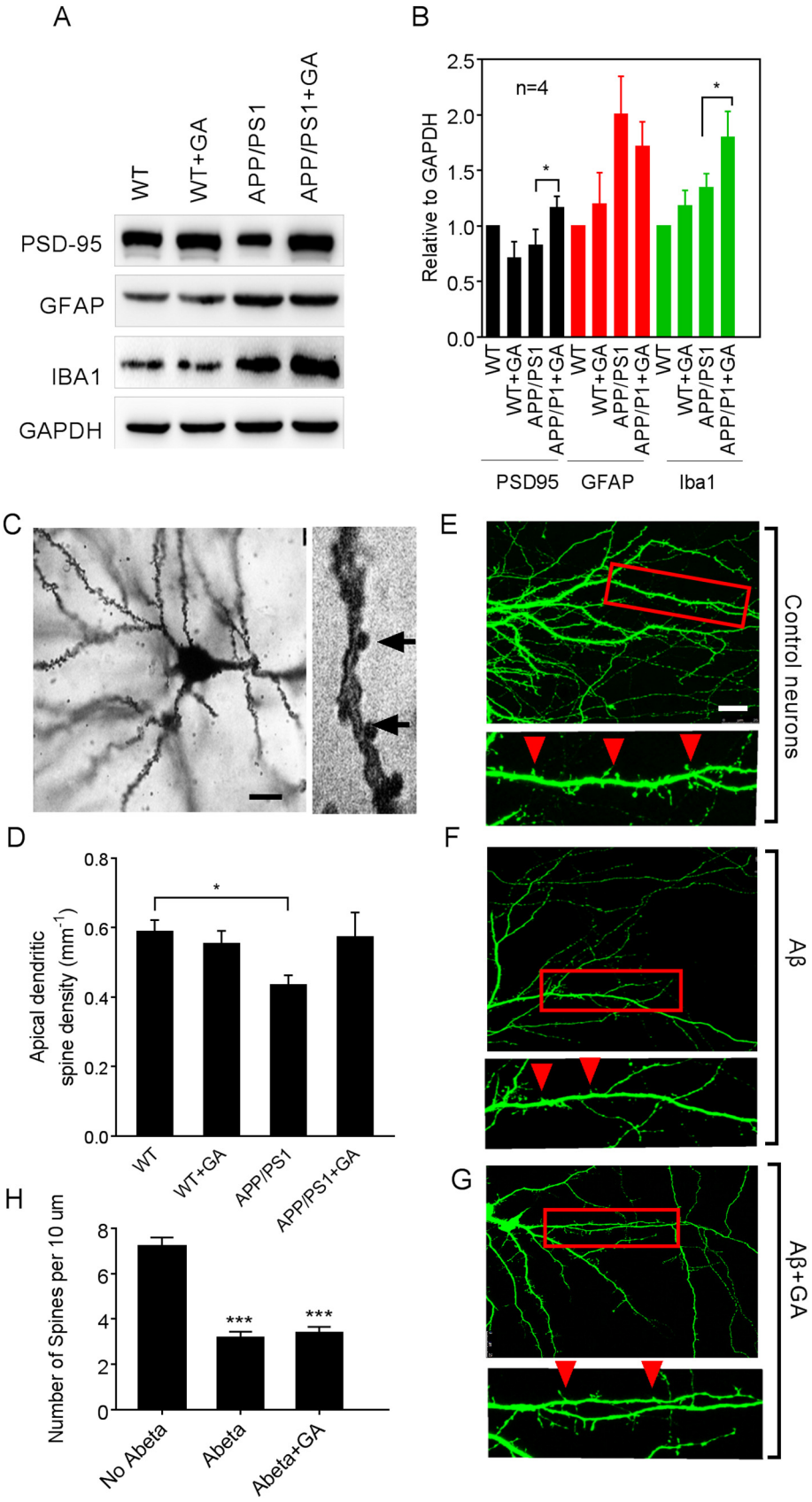

Fig. 3. GA treatment increases synaptic plasticity. The 9-month-old APP/PS1 wildtype and transgenic mouse brain with or without GA treatment were subjected to protein extraction for Western blotting (A) and quantification analysis (B). Antibodies to PSD95, GFAP and IBA1 were used as described in the Method Section. GAPDH was used as an internal control for quantification of the relative expression levels of these genes as shown in panel B ($n = 4$). Thick brain slices (200–250 μm) were subjected to Golgi-Cox staining (C, D). The number of apical dendritic spines indicated in panel C (arrows) were counted and plotted in panel D. To demonstrate directly GA's effect, cultured GFP transgenic mouse cortical neurons expressing endogenous GFP were treated with oligomeric $A\beta_{1-42}$ for 24 h with or without GA treatment (Panels E-G). The dendritic spines were examined under confocal microscopy. The higher magnificent images selected from the respective boxes (red-colored boxes) were also shown underneath each photos. The number of spines per 10 μm of dendrites were plotted in panel H. scale bars = 50 μm. $^{*}p < 0.05$; $^{***}p < 0.01$ by Mann-Whitney *U* test. (For interpretation of the references to color in this figure legend, the reader is referred to the web version of this article.)

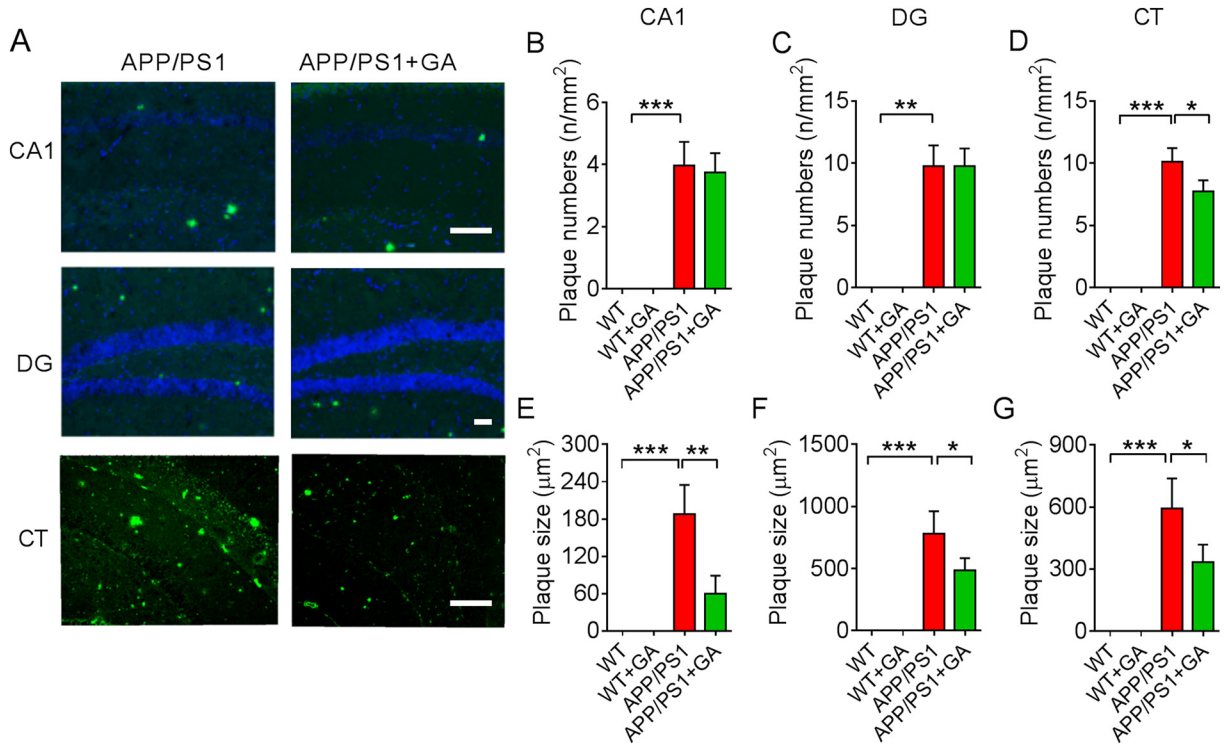

Fig. 4. GA reduced the $A\beta_{1-42}$ plaque size in hippocampus and cortex of 10-month-old APP/PS1 mice. (A) Representative images from the CA1 subfield, dentate gyrus (DG) and cortex (CT) of APP/PS1 and GA-treated APP/PS1 mice, which were stained using ThS to show Aβ plaques. (B–D) Aβ plaque numbers and (E–G) sizes in different regions were measured and quantitatively analyzed using Image J. Data represent mean ± SEM with $n = 3$ in each group. *$p < 0.05$, **$p < 0.01$, ***$p < 0.001$. Scale bars = 500 μm.

3.6. GA attenuates [$(Ca^{2+})i$] induction caused by oligomeric $A\beta_{1-42}$ in cultured cortical neurons

It is known that oligomeric $A\beta_{1-42}$ can induce intracellular calcium [$(Ca^{2+})i$] influx in cultured cortical neurons resulting in neuronal death (Demuro et al., 2005). Therefore, the following experiments were designed to establish the dose-response relationship of [$(Ca^{2+})i$] changes in response to oligomeric $A\beta_{1-42}$, and to determine whether GA treatment can reduce oligomeric $A\beta_{1-42}$ toxicity to neurons through inhibiting [$(Ca^{2+})i$] changes.

First, $A\beta_{1-42}$ peptide was polymerized *in vitro* as described in the Methods section to form oligomeric $A\beta_{1-42}$. When added to the cultured neurons, ratiometric calcium imaging technique was used to show a dose-dependent increase in [$(Ca^{2+})i$] (Fig. 6A). The dose-dependent relationship was determined in Fig. 6B with the $EC_{50} = 2.73 \pm 1.047$ μM. This experiment allowed the establishment of 2.5 μM $A\beta_{1-42}$ as a working concentration for the oligomeric $A\beta_{1-42}$ toxicity studies.

Second, inhibitors to NMDA receptors (MK801) and AMPA receptors (CNQX) were used to determine if they can block $A\beta_{1-42}$ induced [$(Ca^{2+})i$] influx. As shown in Fig. 6C, compared to the level of [$(Ca^{2+})i$] influx caused by 2.5 μM $A\beta_{1-42}$, MK801 (10 μM) inhibited about 40% of that, while CNQX (10 μM) inhibited < 20% of that, indicating that [$(Ca^{2+})i$] in neurons are through multiple channels in response to $A\beta_{1-42}$. Furthermore, extracellular calcium is the main source for the increase of [$(Ca^{2+})i$] level seen in response to Aβ, as bathing neurons in calcium-free solutions showed no [$(Ca^{2+})i$] influx (not shown).

GA attenuated oligomeric $A\beta_{1-42}$-induced [Ca^{2+}]i in cultured cortical neurons and reduced neurotoxicity. To determine whether GA inhibits oligomeric Aβ-induced [$(Ca^{2+})i$] influx to neurons, cultured cortical neurons were treated with 2.5 μM oligomeric $A\beta_{1-42}$ pre-mixed with GA (Fig. 6D,E). From Fig. 6D, it was clear that addition of oligomeric 2.5 μM $A\beta_{1-42}$ elicited a fast and significant increase in [$(Ca^{2+})i$] influx to neurons, while GA with concentration ratios to Aβ at both 1:1 and 1:2 rapidly and significantly reduced [$(Ca^{2+})i$] influx into neurons. The inhibition by GA was about 50% of the [$(Ca^{2+})i$] influx level caused by $A\beta_{1-42}$ without GA (Fig. 6E). Moreover, GA was also not effective in blocking [$(Ca^{2+})i$] influx elicited by treatments with glutamate at 25 μM or 100 μM (Fig. 6F). These studies strongly suggest that GA was effective mainly at the level of reducing the polymerization of toxic $A\beta_{1-42}$, rather than at the level of selectively blocking calcium channel activities.

3.7. Molecular modeling and simulations of GA interaction with $A\beta_{1-42}$

3.7.1. Non-covalent interactions

In order to provide a structural insight of GA interaction with $A\beta_{1-42}$ aggregation, GA chemical derivatives were made which included 3-hydroxybenzoic acid, pyrogallol, 3,4-dihydroxybenzoic acid, 3,5-dihydroxybenzoic acid, and benzoic acid (Fig. 7A). ThT fluorescence assay was used to determine whether these derivatives disrupt $A\beta_{1-42}$ aggregation. As shown in Fig. 7(B and C), GA and pyrogallol significantly reduced Aβ aggregation-induced ThT fluorescence. In contrast, the rest of the GA derivatives were less effective (Fig. 7C), suggesting that the three hydroxyl groups were essential in GA interaction with $A\beta_{1-42}$ aggregates.

The crystal structure of fibrillar $A\beta_{1-42}$ (PDB: 2MXU) is a S-shaped triple-β-motif, which is stabilized by a salt bridge between Lys28 and Ala42 residues. Docking studies revealed that the carboxylic acid group of GA forms hydrogen bond interactions with Lys28 and Ala42 residues, and these interactions were stabilized by hydrogen bonding with Val40 and hydrophobic interactions with Ile41 and Val39 residues (Fig. 7D). The hydrogen bonding interactions between GA and Lys28 and Ala42 residues might break the salt bridge between Lys28 and Ala42, resulting in instability of fibrillar $A\beta_{1-42}$, and ultimately lead to disaggregation of

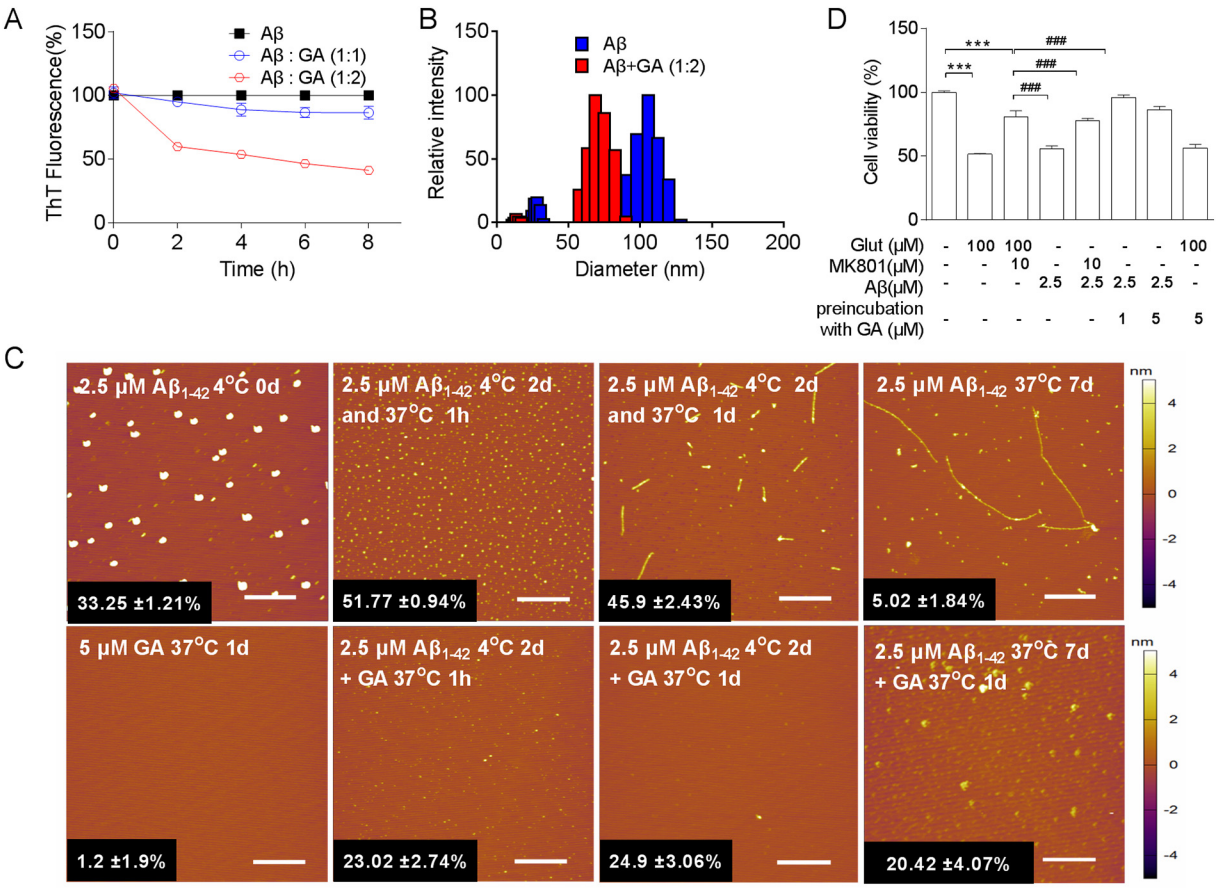

Fig. 5. GA reduced fibrillar $A\beta_{1-42}$ aggregation and toxicity to neurons. GA at the specified concentrations were mixed with the pre-aggregated $A\beta_{1-42}$ before the ThT fluorescence assay (A). (B) DLS assay was also performed to show GA reduction of $A\beta_{1-42}$ aggregate particle sizes at the specified concentration (1:2). (C) Top panel show AFM images of fibrillar $A\beta_{1-42}$ development following incubation at 4 °C and 37 °C. The bottom panels show GA effectively disrupted the formation of $A\beta_{1-42}$ fibrils. Neuronal viability was determined using CCK8 Viability Assay Kit. Number in the black box of each panel in C refers to neuronal death rate caused by the corresponding $A\beta_{1-42}$ mixture. (D) Pre-incubation with GA also reduced the cytotoxicity caused by $A\beta_{1-42}$. Glutamate induced neuronal death and MK801 protection were used as internal controls. GA was not effective in blocking $A\beta_{1-42}$ toxicity to neurons (D). All data sets were $n = 3$. Values represented as mean ± SEM. Scale bars = 30 μm.

$A\beta_{1-42}$ fibrils.

Although hydrogen bonding interactions were observed between benzoic acid and residues Lys28 and Ala42, no additional hydrogen bonding interaction was formed with other residues. Thus, interaction between benzoic acid and Lys28 and Ala42 may be not potent enough to break the salt bridge (Fig. 7F). This suggests that the three hydroxyl groups play a role in stabilizing GA interaction with Aβ aggregation while the presence of the –COOH group is critical in destabilizing the $A\beta_{1-42}$ fibrils.

Pyrogallol has additional binding sites on fibrillar $A\beta_{1-42}$. Hydrogen bonding interactions were observed between pyrogallol and Asn27 and Ala30 residues (Fig. 7E). In addition, Van der Waal interactions with Phe19, Phe20, Ile31 and Ile41 residues were also observed (Fig. 7E). Indeed, the crystal structure of fibrillar $A\beta_{1-42}$ revealed that the inter-chain hydrogen bonding between residue Asn27 is important for the aggregation and fibrils formation. Therefore, the stable hydrogen bonding interaction between pyrogallol and residue Asn27 may explain the disaggregation effect of pyrogallol on fibrillar $A\beta_{1-42}$.

3.7.2. *Covalent interactions*

Another possible disaggregation mechanism of GA derivatives may be through covalent modification. As shown in Fig. 7G, GA and pyrogallol contain a catechol moiety which is easily oxidized to quinone and is susceptible to form covalent interaction with one or more lysine residues on $A\beta_{1-42}$ *via* Schiff-base formation. This covalent interaction will disaggregate the fibrillar $A\beta_{1-42}$. To demonstrate this interaction, a covalent docking of GA quinone and pyrogallol quinone in monomers with $A\beta_{1-42}$ was performed. As shown in Fig. 7H and Fig. 7I, both the oxidized product of GA and pyrogallol covalently interacted with $A\beta_{1-42}$ through Schiff-base formation between the carbonyl group of the oxidized product and ε-amino group of Lys16. The van der Waals interactions between phenyl group of oxidized products and residues Phe20 and Phe19 contributed to the covalent modification. In addition, GA quinone forms an electrostatic interaction with His13. This may explain the lower activity of 3,4-dihydroxybenzoic acid than that of GA, as there is no hydroxyl group in the oxidized product of 3,4-dihydroxybenzoic acid, which means no hydrogen bonding interaction with His13 can be formed. These docking results also revealed that the oxidized product of GA and pyrogallol may be susceptible to form covalent interactions with Lys16, but not the Lys28 residue. We assumed that this may be due to the van der Waals interactions and electrostatic interaction with residues that are adjacent to Lys16.

4. Discussion

The present study systemically analyzed GA's direct beneficial effect on alleviating the cognitive decline of APP/PS1 transgenic mouse. The efficacy of GA was shown in two stages of AD pathology indicating GA is effective to prevent and treat AD. Improvement of synaptic strength of 10-month-old APP/PS1 mouse after GA treatment was associated

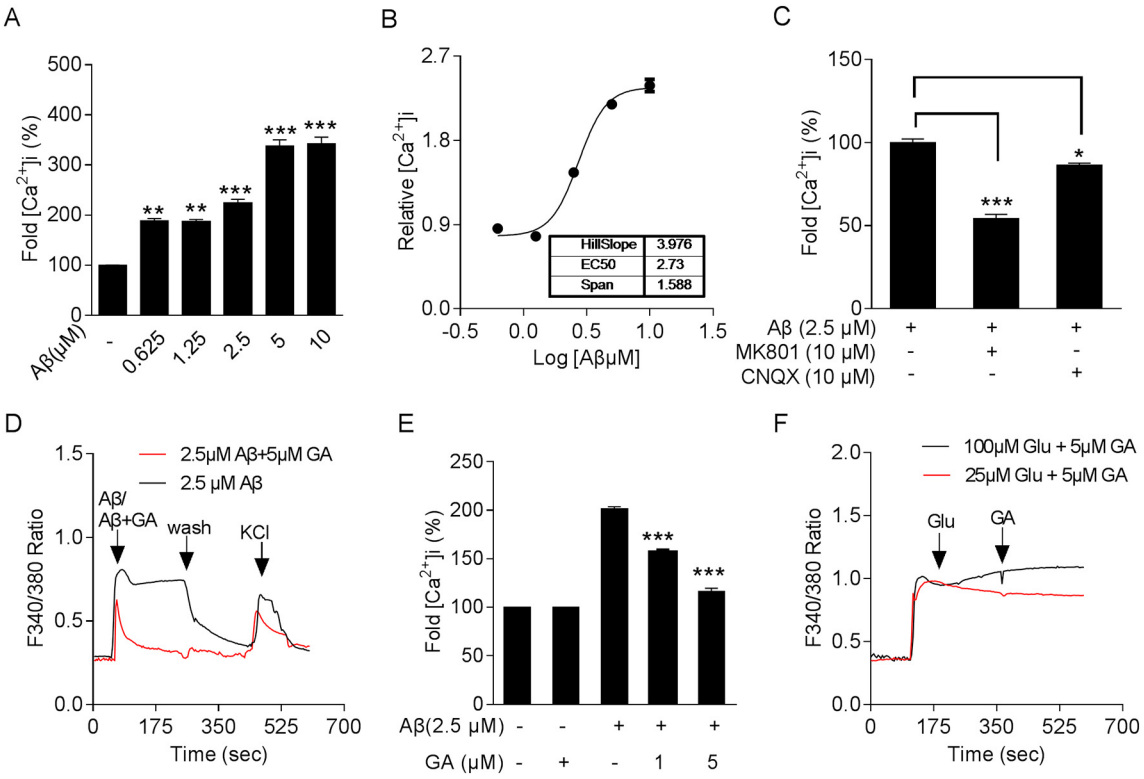

Fig. 6. $A\beta_{1-42}$ elicited increased intracellular calcium in primary cortical neurons. (A) Ratiometric calcium imaging measurement of the level of intracellular calcium ($[Ca^{2+}]i$) in response to $A\beta_{1-42}$ at doses ranging from 0.625 μM to 10 μM. The relative $[Ca^{2+}]i$ level of $A\beta_{1-42}$ treatment was normalized to the baseline calcium level of non-treated cortical neurons. Data represents the average of measurements of at least 20 cells. (B) Concentration-response relationship for $A\beta_{1-42}$-induced $[Ca^{2+}]i$ was determined and the concentration-response curve was fitted using the logistic equation. The EC_{50} was determined to be at 2.73 ± 1.047 μM and the slope factor of 3.976 ± 0.9103. (C) Cultured cortical neurons were treated with 2.5 μM of the oligomeric form of $A\beta_{1-42}$. Fold reduction of $[Ca^{2+}]i$ in neurons treated with 10 μM MK801 or 10 μM CNQX in response to $A\beta_{1-42}$-induced $[Ca^{2+}]i$ was measured. (D) Representative traces of $[Ca^{2+}]i$ in cortical neurons treated with oligomeric $A\beta_{1-42}$ (2.5 μM) (black colored line), or with pre-mixed GA with oligomeric Aβ at a ratio of 2:1 (5 μM: 2.5 μM). A brief wash with PBS removed the increase of $A\beta_{1-42}$-induced $[Ca^{2+}]i$ in neurons. Addition of KCl showed a large increase in $[Ca^{2+}]i$ confirming that these neurons were functional cells. (E) Cultured cortical neurons were treated with oligomeric $A\beta_{1-42}$ (2.5 μM) pre-mixed with GA at 37 °C for at least 15 min before measuring $A\beta_{1-42}$-induced $[Ca^{2+}]i$ in neurons. (F) Cultured cortical neurons were treated with 25 μM or 100 μM glutamate followed by the addition of GA, which did not inhibit glutamate-induced calcium influx. Data represent mean ± SEM with $n = 20$ cells in each group. ** $p < 0.01$, *** $p < 0.001$.

with the reduction of Aβ plaque size (but not numbers) in the brain, indicating GA may shrink plaques. Indeed, series of *in vitro* analyses showed that GA disrupts $A\beta_{1-42}$ aggregation thereby reducing neurotoxicity. Molecular docking studies indicated that the three hydroxyl groups of GA are essential in stabilizing the interaction of GA with $A\beta_{1-42}$ aggregation. Benzoic acid, a GA derivative lacking of the three hydroxyl groups, was ineffective. All data supports the idea that GA is an effective compound for treating AD.

Several previously published studies on GA's role in AD used either *in vitro* cultured cells or AD models lacking of physiological relevance (Ferruzzi et al., 2009; Hajipour et al., 2016; Jayamani and Shanmugam, 2014; Kim et al., 2011; Kim, 2007; Kroes et al., 1992; Liu et al., 2013). The APP/PS1 transgenic mouse is an excellent model system to determine the development of cognitive impairments in mice over time (Gotz et al., 2018). The 4-month-old APP/PS1 mouse has very small amount of Aβ plaque deposition in the brain (low plaque stage) with mild cognitive deficits in the spatial reference and working memories, resembling those seen during early stage of human AD development. In contrast, the 9-month-old APP/PS1 transgenic mice carrying a large amount of $A\beta_{1-42}$ plaques in the brain (high plaque stage) show severely compromised cognitive functions, representing the late stage of AD seen in humans. One of the most interesting findings of the present study was that GA not only significantly improved cognitive deficits of the 4-month-old APP/PS1 mice, but also significantly ameliorated cognitive deficits of the 9-month-old AD mice, suggesting GA can be used to prevent and treat AD. Our study lends support to the findings reported by Mori et al. (2017) that octyl gallate, which is metabolized to GA in the gut, can improve cognition and neurodegeneration in APP/PS1 transgenic mouse.

Enhancing synaptic strength is a key indicator of GA's effect. Hippocampal LTP is considered one of the major cellular mechanisms underlying learning and memory. The 9-month-old APP/PS1 mice (plus one month GA treatment) exhibited a significantly reduced LTP compared to those of the WT littermates and GA-treated mice (Fig. 3). This difference in LTP proved GA's role in enhancing synaptic strength of APP/PS1 mouse brain. Indeed, expressions of several synaptic marker proteins, such as PSD95 and synaptophysin (not shown), were also significantly increased in GA-treated mouse brain. Using an *in situ* injection of $A\beta_{1-42}$ to rat hippocampus model, GA was also found to enhance LTP (Hajipour et al., 2016), which supports the argument that GA can indeed be beneficial to the long-term improvement of cognitive functions of AD.

GA's ability to reduce Aβ aggregation is demonstrated using *in vitro* assays as shown in Fig. 5. The combination of data from assays of ThT, AFM, DLS and neuronal viability indicated that GA significantly reduced $A\beta_{1-42}$ aggregation and neuronal toxicity (Fig. 5C). These results support the *in vivo* observation that GA shank plaque size and reduced neurotoxicity. Published studies showed that GA inhibits kappa-casein fibril formation and stabilizes kappa-casein to prevent its aggregation (Liu et al., 2013). Incubation of gallic acid with preformed $A\beta_{1-40}$ amyloid fibrils produced a time- and dose-dependent decrease in fibril-induced ThT fluorescence which was not due to gallic acid competition

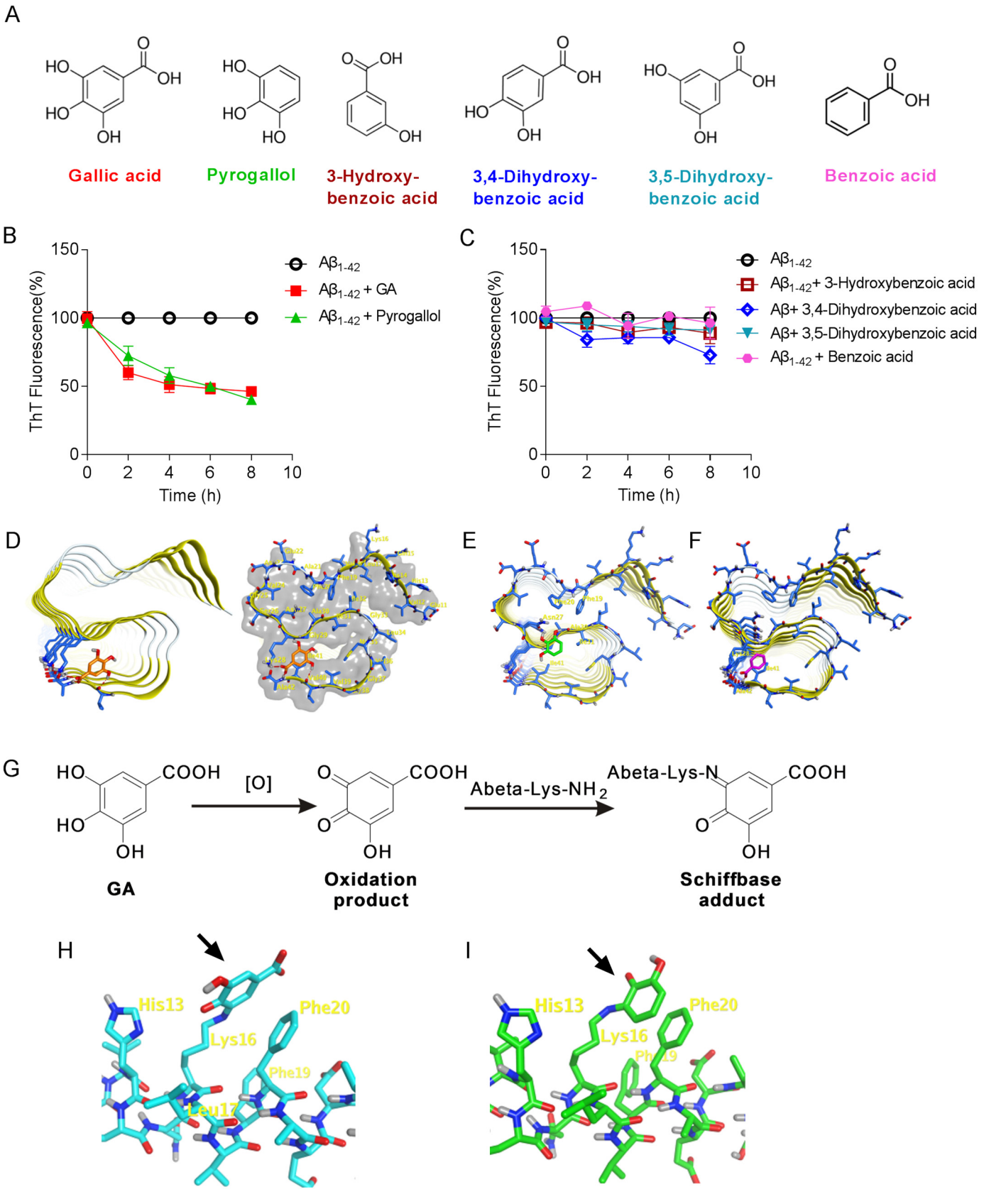

(caption on next page)

Fig. 7. Structures of GA derivative (A) and their effects in reducing ThT fluorescence intensity (B, C). The predicted docking modes to fibrillar $A\beta_{1-42}$ are shown in panels D-I. GA derivative structures are shown in (A), where GA is in orange color; pyrogallol (benzene-1,2,3-triol) in green color; 3-hydroxybenzoic acid in brown color; 3,4-dihydroxybenzoic acid in blue color; 3,5-dihydroxybenzoic acid in pale turquoise color; benzoic acid in pink color. GA derivatives effect in reducing ThT fluorescence derived from $A\beta_{1-42}$ aggregation (as 100%) is shown in (B) and (C) for clarity. Pyrogallol has similar potency to GA in reducing ThT fluorescence derived from $A\beta_{1-42}$ aggregation (B), while all others were less effective in comparison (C). (D) Predicted binding modes of GA in the crystal structure of fibrillar $A\beta_{1-42}$ shown as S-shaped triple-β-motif (PDB: 2MXU,) using the MOE software. GA is shown as orange colored stick; hydrogen bonding is represented as a red dash; $A\beta_{1-42}$ is represented as yellow cartoon. Predicted noncovalent binding modes of pyrogallol (E, green sticks) and benzoic acid (F, pink sticks) in the aggregated structure of fibrillar $A\beta_{1-42}$ (PDB: 2MXU) using the MOE software. (G) The oxidation product of GA derivatives and the proposed Schiff base adduct. Covalent docking of oxidized product of GA (H, black colored arrow) and pyrogallol (I, black colored arrow) with $A\beta_{1-42}$ (PDB: 1IYT) through a Schiff-base formation between the carbonyl group of the oxidized product and ε-amino group of Lys16. Covalent docking was conducted with DOCKTITE program in the MOE software. (For interpretation of the references to color in this figure legend, the reader is referred to the web version of this article.)

with the fluorophore (LeVine 3rd et al., 2012). The inhibition of α-synuclein fibrillation, toxicity and disaggregation of preformed α-synuclein amyloid fibrils also occurred following GA treatment (Ardah et al., 2014; Di Giovanni et al., 2010). Together these studies all support a role of GA in dissociation of $A\beta_{1-42}$ aggregation and detoxification.

How dose GA reduce $A\beta_{1-42}$ aggregation remains unclear. There are several possibilities. One, GA binds to soluble, non-toxic oligomers with no β-sheet content, thereby stabilizing their structure and may remodel fibrils into non-toxic oligomers (LeVine 3rd et al., 2012). GA remodeling of oligomers may represent a potential mechanism of action. Second, Structure activity relationship data obtained from fourteen structurally similar benzoic acid derivatives showed that the inhibition of α-synuclein fibrillation by GA is related to the number of hydroxyl moieties and their position on the phenyl ring (Ardah et al., 2014). Indeed, based on our atomic scale modeling studies and the ThT assay results, our data confirmed that the three hydroxyl groups of GA are essential in stabilizing the interaction of GA with $A\beta_{1-42}$ aggregation. The –COOH group of GA appears to be essential in inhibiting the $A\beta_{1-42}$ fibril formation. GA potentially disrupts the salt bridge between the residues of Lys28-Ala42 through non-covalent chemical bonding. Alternatively, oxidized GA and pyrogallol covalently interact with $A\beta_{1-42}$ through Schiff-base formation between carbonyl group of the oxidized product and the ε-amino group of Lys16. Both interactions potentially alter the lateral association of layers of $A\beta_{1-42}$ and prevent further $A\beta_{1-42}$ aggregation. Interestingly, none of the benzoic acid–related compounds had any effect on $A\beta_{1-40}$ amyloid fibrils ThT fluorescence even after several hours of incubation (LeVine 3rd et al., 2012), supporting our findings on $A\beta_{1-42}$ amyloid fibrils.

Despite of lacking the understanding of GA's precise molecular mechanisms, association of modulation of secretase activities, and attenuation of inflammation by these small molecules have been proposed (Mori et al., 2017; Mori et al., 2012). GA has activities such as anti-oxidation, scavenging free radicals, anti-inflammation, anti-microbial and anti-cancer (Isuzugawa et al., 2001; Kim et al., 2011; Kim, 2007; Kroes et al., 1992). Our data showed that GA-treated APP/PS1 mouse increased microglial activation (IBA1 expression) and reduced inflammatory response (GFAP expression) supports the proposed mechanisms. Whether the reduced inflammatory response was due to reduction in the amount of $A\beta_{1-42}$ aggregation present in the brain following GA treatment, or due to GA's direct anti-inflammatory role remains to be determined.

Another potential avenue to explain GA's action is shown in Fig. 6. Mixing GA with $A\beta_{1-42}$ fibrils reduced $A\beta_{1-42}$-induced intracellular calcium influx to about half of that without GA treatment as shown in Fig. 6 panel D, indicating GA partially blocks Aβ-induced intracellular calcium influx and neurotoxicity. It was previously unknown as to whether GA has any effect on calcium channel functions. Because NMDA receptor-mediated calcium influx is one of the major mechanisms of neuronal toxicity in many neurological diseases including AD, it has been shown that uncompetitive blockers of NMDA receptor-mediated intracellular calcium influx, such as memantine, confer potent protection against AD (Chen and Lipton, 1997; Lipton and Chen, 2004). We therefore investigated the effect of GA on $A\beta_{1-42}$ induced calcium changes. As shown in Fig. 6C, MK801 and CNQX, antagonists for NMDA and AMPA receptors, respectively, only inhibited < 50% and 20% of the calcium influx, respectively, confirming the existence of additional calcium channels formed by $A\beta_{1-42}$. The oligomerized and aggregated forms of $A\beta_{1-42}$ can form calcium channels to disrupt intracellular calcium homeostasis and cause neurotoxicity (Demuro et al., 2010). GA did not block glutamate-induced intracellular calcium influx. These studies strongly suggest that GA reduces Aβ-mediated calcium influx was mainly at the level of reducing $A\beta_{1-42}$ aggregation and its associated calcium channel forming capabilities. The fact that GA was not effective in blocking $[(Ca^{2+})i]$ influx elicited by glutamate at 25 μM or 100 μM (Fig. 6F), further supports the argument that the point of action for GA was not at the calcium channel level.

In spite of ample circumstantial evidence showing beneficial effects of polyphenolic compounds in reducing the onset of AD, the molecular mechanisms remain elusive. Together we show that GA may have multiple targets including inhibit Aβ aggregation, increase synaptic strength, reduce inflammation and partially block intracellular calcium influx. These data shed new light on possible mechanisms of GA function and support the view that GA is a promising drug candidate to delay and treat AD in humans. Future studies of GA's clinical benefits are warranted.

Acknowledgments

We thank SUSTech Animal Facility for the maintenance of transgenic mice. Financial supports to Dr. Sheng-Tao Hou were from grants from the National Natural Science Foundation of China (81571287, 81871026), Guangdong Natural Science Foundation (2017A030313808), Shenzhen Science and Technology Innovation Committee Basic Science Research Grants (JCYJ20140417105742709, JCYJ20160301112230218); State Key Laboratory of Neuroscience Open Competition Grants (SKLN-201403), SUSTech Peacock Program Start-up Fund (22/Y01226109) and SUSTech Brain Research Centre Fund. STH is also supported by the Guangdong Innovation Platform of Translational Research for Cerebrovascular Diseases, Financial support to Dr. Jing Xu and Dr. Chengqing Ning came from the National Natural Science Foundation of China (No. 21402082, No. 21772082 and No. 21702094), SZSTI (Pu20150267, Ji20170314 and Peacock Tech-Innovation 2018), and SZDRC (K16205905).

Conflict of interest

Authors declare no conflict of interests.

Authors contributions

MY and ZZ performed animal breeding, genotyping, behavioral studies, analyzed the data and wrote the first draft of the paper. XWC carried out neuronal cultures, AFM, ThT assay and calcium imaging studies; JHL did LTP recordings and brain slices; HC, LZ, and SY are responsible for the initial studies of Aβ aggregation, ThT assay, and dendritic studies; TMG was responsible for supervising the LTP studies, CQN and JX carried out molecular docking studies, and STH conceived the idea, provided financial support to the project, discussed the data

and analyzed the results. STH revised the first draft and wrote the manuscript.

Supplementary data

Supplementary data to this article can be found online at https://doi.org/10.1016/j.nbd.2018.11.009.

References

Ardah, M.T., et al., 2014. Structure activity relationship of phenolic acid inhibitors of alpha-synuclein fibril formation and toxicity. Front. Aging Neurosci. 6, 197.

Barrett, A.D., et al., 2010. New vaccine development for chronic brain disease. Neuropsychopharmacology 35, 354.

Bezprozvanny, I., Mattson, M.P., 2008. Neuronal calcium mishandling and the pathogenesis of Alzheimer's disease. Trends Neurosci. 31, 454–463.

Chen, H.S., Lipton, S.A., 1997. Mechanism of memantine block of NMDA-activated channels in rat retinal ganglion cells: uncompetitive antagonism. J. Physiol. 499, 27–46 Pt 1.

Demuro, A., et al., 2005. Calcium dysregulation and membrane disruption as a ubiquitous neurotoxic mechanism of soluble amyloid oligomers. J. Biol. Chem. 280, 17294–17300.

Demuro, A., et al., 2010. Calcium signaling and amyloid toxicity in Alzheimer disease. J. Biol. Chem. 285, 12463–12468.

Di Giovanni, S., et al., 2010. Entacapone and tolcapone, two catechol O-methyltransferase inhibitors, block fibril formation of alpha-synuclein and beta-amyloid and protect against amyloid-induced toxicity. J. Biol. Chem. 285, 14941–14954.

Diaz, J.C., et al., 2009. Small molecule blockers of the Alzheimer Abeta calcium channel potently protect neurons from Abeta cytotoxicity. Proc. Natl. Acad. Sci. U. S. A. 106, 3348–3353.

Du, W.J., et al., 2015. Brazilin inhibits amyloid beta-protein fibrillogenesis, remodels amyloid fibrils and reduces amyloid cytotoxicity. Sci. Rep. 5, 7992.

Ferruzzi, M.G., et al., 2009. Bioavailability of gallic acid and catechins from grape seed polyphenol extract is improved by repeated dosing in rats: implications for treatment in Alzheimer's disease. J. Alzheimers Dis. 18, 113–124.

Forner, S., et al., 2017. Synaptic impairment in Alzheimer's disease: a dysregulated symphony. Trends Neurosci. 40, 347–357.

Gotz, J., et al., 2018. Rodent models for Alzheimer disease. Nat. Rev. Neurosci. 10, 583–598.

Gravina, S.A., et al., 1995. Amyloid beta protein (A beta) in Alzheimer's disease brain. Biochemical and immunocytochemical analysis with antibodies specific for forms ending at A beta 40 or A beta 42(43). J. Biol. Chem. 270, 7013–7016.

Haass, C., et al., 1995. The Swedish mutation causes early-onset Alzheimer's disease by beta-secretase cleavage within the secretory pathway. Nat. Med. 1, 1291–1296.

Hajipour, S., et al., 2016. Effect of gallic acid on dementia type of Alzheimer disease in rats: electrophysiological and histological studies. Basic Clin. Neurosci. 7, 97–106.

Han, Z., et al., 2013. Fast, non-competitive and reversible inhibition of NMDA-activated currents by 2-BFI confers neuroprotection. PLoS One 8, e64894.

Hardy, J., Selkoe, D.J., 2002. The amyloid hypothesis of Alzheimer's disease: progress and problems on the road to therapeutics. Science 297, 353–356.

Herline, K., et al., 2018. Recent advancements toward therapeutic vaccines against Alzheimer's disease. Expert Rev. Vaccines 17, 707–721.

Hou, S.T., et al., 2006. Calpain-cleaved collapsin response mediator protein-3 induces neuronal death after glutamate toxicity and cerebral ischemia. J. Neurosci. 26, 2241–2249.

Hou, S.T., et al., 2013. Collapsin response mediator protein 3 deacetylates histone H4 to mediate nuclear condensation and neuronal death. Sci. Rep. 3, 1350.

Hou, S.T., et al., 2015. Semaphorin3A elevates vascular permeability and contributes to cerebral ischemia-induced brain damage. Sci. Rep. 5, 7890.

Hou, S.T., et al., 2016. Phaseic acid, an endogenous and reversible inhibitor of glutamate receptors in mouse brain. J. Biol. Chem. 291, 27007–27022.

Hudson, S.A., et al., 2009. The thioflavin T fluorescence assay for amyloid fibril detection can be biased by the presence of exogenous compounds. FEBS J. 276, 5960–5972.

Hughes, R.N., 2004. The value of spontaneous alternation behavior (SAB) as a test of retention in pharmacological investigations of memory. Neurosci. Biobehav. Rev. 28, 497–505.

Isuzugawa, K., et al., 2001. Catalase contents in cells determine sensitivity to the apoptosis inducer gallic acid. Biol. Pharm. Bull. 24, 1022–1026.

Ittner, L.M., et al., 2010. Dendritic function of tau mediates amyloid-beta toxicity in Alzheimer's disease mouse models. Cell 142, 387–397.

Jankowsky, J.L., et al., 2001. Co-expression of multiple transgenes in mouse CNS: a comparison of strategies. Biomol. Eng. 17, 157–165.

Jayamani, J., Shanmugam, G., 2014. Gallic acid, one of the components in many plant tissues, is a potential inhibitor for insulin amyloid fibril formation. Eur. J. Med. Chem. 85, 352–358.

Jiang, S.X., et al., 2007. Neuropilin-1 is a direct target of the transcription factor E2F1 during cerebral ischemia-induced neuronal death in vivo. Mol. Cell. Biol. 27, 1696–1705.

Kalaria, R.N., et al., 2008. Alzheimer's disease and vascular dementia in developing countries: prevalence, management, and risk factors. Lancet Neurol. 7, 812–826.

Kayed, R., et al., 2011. Alzheimers disease: review of emerging treatment role for intravenous immunoglobulins. J. Cent. Nerv. Syst. Dis. 3, 67–73.

Kim, Y.J., 2007. Antimelanogenic and antioxidant properties of gallic acid. Biol. Pharm. Bull. 30, 1052–1055.

Kim, M.J., et al., 2011. Gallic acid, a histone acetyltransferase inhibitor, suppresses beta-amyloid neurotoxicity by inhibiting microglial-mediated neuroinflammation. Mol. Nutr. Food Res. 55, 1798–1808.

Kocis, P., et al., 2017. Elucidating the Abeta42 anti-aggregation mechanism of action of tramiprosate in Alzheimer's disease: integrating molecular analytical methods, pharmacokinetic and clinical data. CNS Drugs 31, 495–509.

Korczyn, A.D., 2008. The amyloid cascade hypothesis. Alzheimers Dement. 4, 176–178.

Kroes, B.H., et al., 1992. Anti-inflammatory activity of gallic acid. Planta Med. 58, 499–504.

Kurt, M.A., et al., 2001. Neurodegenerative changes associated with beta-amyloid deposition in the brains of mice carrying mutant amyloid precursor protein and mutant presenilin-1 transgenes. Exp. Neurol. 171, 59–71.

Lagadec, S., et al., 2012. Early temporal short-term memory deficits in double transgenic APP/PS1 mice. Neurobiol. Aging 33 (203), e1–11.

Leger, M., et al., 2013. Object recognition test in mice. Nat. Protoc. 8, 2531–2537.

LeVine 3rd, H., et al., 2012. Dihydroxybenzoic acid isomers differentially dissociate soluble biotinyl-Abeta(1-42) oligomers. Biochemistry 51, 307–315.

Lipton, S.A., Chen, H.S., 2004. Paradigm shift in neuroprotective drug development: clinically tolerated NMDA receptor inhibition by memantine. Cell Death Differ. 11, 18–20.

Liu, Y., et al., 2013. Gallic acid is the major component of grape seed extract that inhibits amyloid fibril formation. Bioorg. Med. Chem. Lett. 23, 6336–6340.

Liu, J.H., et al., 2015. Social isolation during adolescence strengthens retention of fear memories and facilitates induction of late-phase long-term potentiation. Mol. Neurobiol. 52, 1421–1429.

Mattson, M.P., et al., 1992. Beta-amyloid peptides destabilize calcium homeostasis and render human cortical neurons vulnerable to excitotoxicity. J. Neurosci. 12, 376–389.

Mori, T., et al., 2012. Tannic acid is a natural beta-secretase inhibitor that prevents cognitive impairment and mitigates Alzheimer-like pathology in transgenic mice. J. Biol. Chem. 287, 6912–6927.

Mori, T., et al., 2017. Combination therapy with octyl gallate and ferulic acid improves cognition and neurodegeneration in a transgenic mouse model of Alzheimer's disease. J. Biol. Chem. 292, 11310–11325.

Scholz, C., et al., 2015. DOCKTITE-a highly versatile step-by-step workflow for covalent docking and virtual screening in the molecular operating environment. J. Chem. Inf. Model. 55, 398–406.

Sengupta, U., et al., 2016. The role of amyloid-beta oligomers in toxicity, propagation, and immunotherapy. EBioMedicine 6, 42–49.

Vorhees, C.V., Williams, M.T., 2006. Morris water maze: procedures for assessing spatial and related forms of learning and memory. Nat. Protoc. 1, 848–858.

Wisniewski, T., Drummond, E., 2016. Developing therapeutic vaccines against Alzheimer's disease. Expert Rev. Vaccines 15, 401–415.